Master's Thesis

Enhancing thermal conductivity of amorphous polymers

Jaekyo Lee

Department of Mechanical Engineering

Graduate School of UNIST

2020

Enhancing thermal conductivity of amorphous polymers

Jaekyo Lee

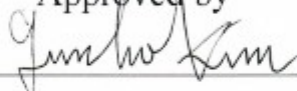Department of Mechanical Engineering

Graduate School of UNIST

Enhancing thermal conductivity of amorphous polymers

A thesis

submitted to the Graduate School of UNIST

in partial fulfillment of the

requirements for the degree of

Master of Science

Jaekyo Lee

07/09/2020 of submission

Approved by

‾‾‾‾‾‾‾‾‾‾‾‾‾‾‾‾‾‾‾‾‾‾‾

Advisor

Gun-ho Kim

Enhancing thermal conductivity of amorphous polymers

Jaekyo Lee
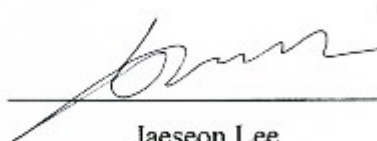
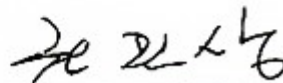This certifies that the thesis of Jaekyo Lee is approved.

07. 09. 2020 of submission

Gun-ho Kim

Jaeseon Lee

Min Sang Kwon

Abstract

High thermal conductivity of polymers is important to improve the functionality and reliability of products by efficiently dissipating heat in polymer products. Several studies have demonstrated that extended polymer chain conformation enhances the heat transfer in amorphous polymers. Here, we demonstrate that the tacticity of polymers alters the chain conformation in ionized polymers due to the difference in the coulombic interaction among the functional groups. Depending on their tacticity, polymers with the similar degree of ionization were observed to have significantly different cross-plane thermal conductivities, as high as 1.14 W/m·K in ionized atactic poly(acrylic acid)(PAA) and 0.69 W/m·K in ionized syndiotactic poly(methacrylic acid)(PMAA) but merely 0.55 W/m·K in ionized isotactic PAA and 0.48 W/m·K in ionized isotactic PMAA and atactic PMAA. Elastic modulus, viscosity data which affects the conformation of the polymer chain, suggested validating effect on the thermal conductivity of polymers.

In addition, we have systematically investigated the effect of annealing temperature on the cross-plane thermal conductivity of an amorphous natural bio-polymer. The results display a systematic increase in thermal conductivity (0.2 W/m·K to 1.3 W/m·K) with annealing temperature. This high thermal conductivity is mainly achieved by improving the crystallinity of polymer and low inter-planar spacing resulted to efficient phonon transport.

Contents

List of Figures

List of Tables

Nomenclature

Abbreviations

AFM	Atomic force microscopy
AIBN	Azobisisobutyronitrile
FT-IR	Fourier-transform infrared spectroscopy
MW	Molecular weight
NMR	Nuclear magnetic resonance
PAA	Polyacrylic acid
PMAA	Polymethacrylic acid
PMMA	Polymethyl methacrylate
PS	Polystyrene
PSD	Phase-sensitive detection
TBDMSMA	Tert-butyldimethylsilyl methacrylate
TCR	Temperature coefficient of resistance
THF	Tetrahydrofuran
TIPSMA	Triisopropylsilyl methacrylate
TRGO	Thermally reduced graphene oxide
XRD	X-ray powder diffraction

Symbol	Description	Unit
D	Thermal diffusivity	$[\text{mm}^2/\text{s}]$
f	Frequency	[Hz]
$I_{h,0}$	Alternating current amplitude	[A]
κ	Cross-plane thermal conductivity	$[\text{W/m} \cdot \text{K}]$
l_h	Length of the heater line	[mm]
P	Power induced by heater line	[W]
R	Resistance of the heater line	[Ω]
R_a	Arithmetical mean deviation of the thickness profile	[nm]
r	Penetration depth	[μm]
T	Temperature difference	[K]
t_f	Thickness of the film	[μm]
$V_{1\omega}$	The first harmonic voltage	[V]
$V_{3\omega}$	The third harmonic voltage	[V]
w_h	Width of the heater line	[mm]

Greek symbols

α	Degree of ionization	[%]
β	Temperature coefficient of resistance	[1/K]
ω	Frequency	[Hz]

I. Introduction

Polymers have been used and studied in various fields, because of their numerous advantages such as lightweight, ease of processing, flexible, transparent, corrosion to resistance, and low cost. Especially, the polymer has recently shown their potential in rechargeable batteries,[1] high energy storage,[2] electromagnetic shielding,[3] electronics packaging,[4] thermal interface materials,[5] and high-power density electronic devices.[6] and others as shown in Figure 1. However, there is a factor that interferes use and development of polymer is their low thermal conductivity. Due to their low thermal conductivity, it cannot dissipate the heat generation inside the products and degrade the performance of the product. Therefore, effective thermal management of polymer devices is highly important to ensure the performance, long term stability, and lifetime. Thus, it is important to develop polymer materials associated with excellent thermal conductivity.

Figure 1. Various applications of polymers.

From the previous studies, to improve the thermal conductivity of polymer, we commonly blend fillers with high thermal conductivity such as metal[7], carbon nanotubes,[8] or graphene flakes.[9] These high k-fillers create a percolation network within the polymer matrix and advanced heat transfer, so that reinforces the thermal conductivity. However, a large load of thermally conducting fillers has to be dispersed to achieve high thermal conductivity, and large loading of filler resulted in high manufacturing costs, heavy weight, and impaired mechanical parameters by difficulty in homogeneous dispersion.

In addition, there were various prior studies that improve thermal conductivity by changing the chain structure. While bulk polymers have a low thermal conductivity, constituent individual chains are expected to show high thermal conductivity. The thermal conductivity of a single polyethylene chain calculated to over 100 W/m·K and should increase with the chain length.[10] The thermal conductivity of

ultra-drawn nanofiber, aligned by the stretching of a polymer chain, was found to be as high as 104 W/m·K[11]. Moreover, the cross-plane thermal conductivity of brushes grafted with poly(3-methyl thiophene) was reported to be higher than 2 W/m·K.[12] Improvement of the interface on enhanced chain conformation led by covalent grafting which shows the effect of reducing energetic and positional disorder, leading to an improved cross-plane thermal conductivity. However, these approaches face problems either in terms of limiting the orientation of chain extension in a particular direction or expanding nanoscale films for practical applications. Although continuous studies are conducted on the mechanisms of thermal transport in amorphous polymers, highly coiled and entangled inter-chain structure, weak nonbonding inter-chain interactions, and loose chain packing with voids[13] are considered to be a factor in inhibiting the thermal conductivity in bulk amorphous polymers.

It has been studied to make high thermal conductivity polymer by transform chain alignment of a pure polymer by mechanical stretching,[14, 15] template-assisted polymer growth,[16, 17] and surface grafting.[12] More recently, incorporating functional groups in polymer blending, strengthened inter-chain bonding of stretches polymer backbone chains were found to be an effective method to improve thermal conductivity in amorphous polymers.[18, 19]
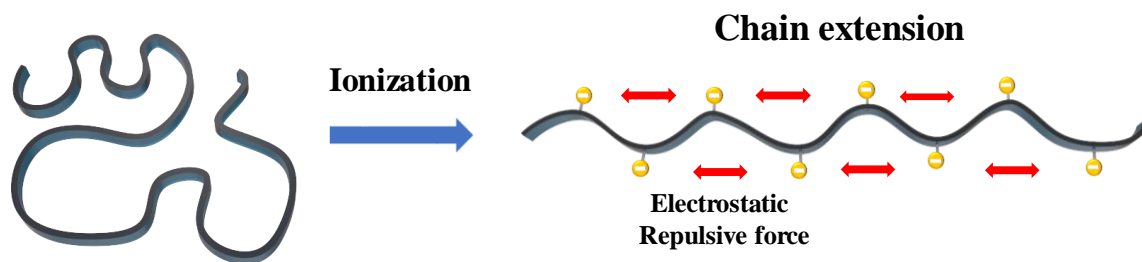
Figure 2. Enhancing thermal conductivity by extended chain conformation.

In particular, there was research about improving polymer thermal conductivity through extended chain conformation by electrostatic repulsion force among ionized functional groups.[19] In this research, they used weak polyelectrolyte poly(acrylic acid)(PAA), which is easy to be ionized with the increase of the solution pH, to show the enhancement in thermal conductivity. As polymer ionized, the concentration of anionic carboxylate groups($-COO^-$) increased, and electrostatic repulsive force among adjacent pendant groups stretches polymer backbone. Meanwhile, extended chain conformation provides longer spatial paths for heat transfer with a larger persistence length, and lead to high thermal conductivity. They showed a dramatic increment in cross-plane thermal conductivity as polymer pH increased, as high as ~1.2 W/m·K, which is almost six times higher than the original polymer. This study showed its strength on enhancing thermal conductivity of polymer without limitations, such as the ratio between blending materials, and the use of special material sets that contribute to improved interchain bonding.
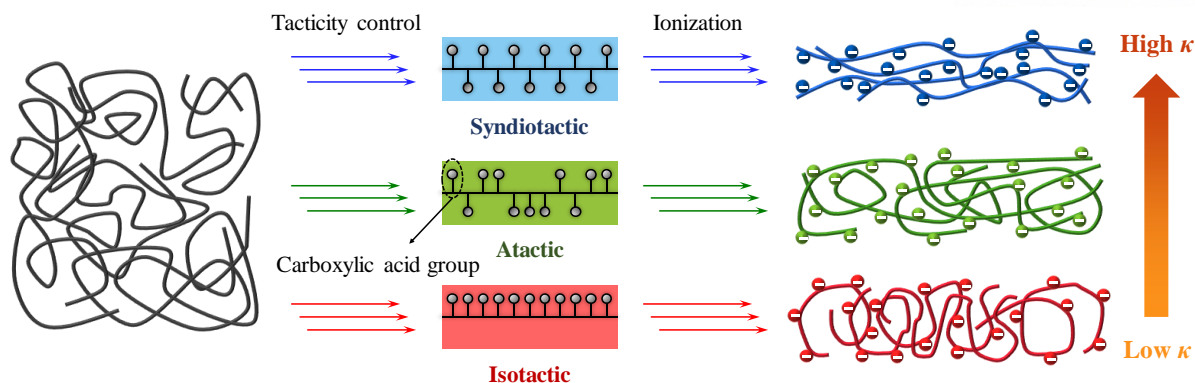
Figure 3. Concept of chain conformation in ionized polyelectrolyte thin films as a tacticity difference.

Base on the above research, here we propose further study about the change of amorphous polymer thermal conductivity according to the difference of chain conformation, depending on the spatial arrangement of the functional groups, which is largely influenced by polymer tacticity. Polymer tacticity is determined by the configurational pendant group among the polymer backbone. In syndiotactic polymers, functional groups have alternate positions along the chain. However, in isotactic polymers, functional groups are located on the same side of the molecule backbone. Accordingly, polymer tacticity affects the conformation of the polymer chain which leading to affect flexibility, stiffness, crystallinity, viscosity,[20, 21] elastic property,[22-24] and thermal conductivity of the polymer. Accordingly, we proposed that a different tacticity in a weak polyelectrolyte shows a difference in electrostatic repulsion force at the highly ionized condition and affects the chain conformation. Thus, the difference in tacticity affects the improvement of the thermal conductivity of the polymer. We anticipated that in syndiotactic polymer, electrostatic repulsive force among the functional groups due to ionization is alternately distributed, which offsetting each other and highly extending the chain conformation. In contrast, isotactic polymer expected to form a curved or entangled chain conformation, with their repulsion force concentrated on only one side, therefore end to end distance of polymer will be much less than other tacticity. Thus, the research was carried with the expectation that the syndiotactic polymer will show superior thermal conductivity enhancement than other tacticities.

R = –H, Syndiotactic PAA
R = –CH₃, Syndiotactic PMAA

R = –H, Atactic PAA
R = –CH₃, Atactic PMAA

R = –H, Isotactic PAA
R = –CH₃, Isotactic PMAA
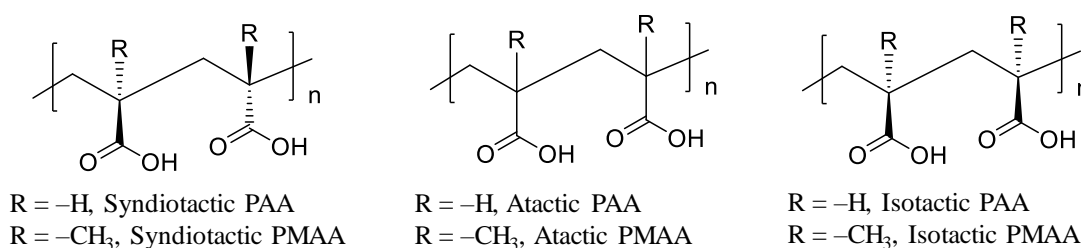
Figure 4. Molecular structure of polyelectrolytes (PAA, PMAA) used in this work.

Here, we experimentally showed the effect of tacticity on the thermal conductivity of the polymer. In particular, we studied the effect of tacticity on the thermal conductivity of ionized poly (methacrylic acid) (PMAA) and poly (acrylic acid) (PAA)(Figure 4). We further measured the viscosity and elastic modulus representing the chain extension to investigate the relation with thermal conductivity. Extended chain conformation through viscosity data showed a strong correlation with elastic modulus data[25], but it did not necessarily lead to an improvement in thermal conductivity. We observed that the polymer tacticity has a strong effect on the thermal conductivity of the ionized polymer. As a result, tacticity had a strong effect on the thermal conductivity of ionized polymers, having as high as 1.14 W/m·K in atactic PAA (*a*-PAA) and 0.69 W/m·K in syndiotactic PMAA (*s*-PMAA) but merely 0.55 W/m·K in isotactic PAA (*i*-PAA) and 0.48 W/m·K in isotactic PMAA (*i*-PMAA) and atactic PMAA (*a*-PMAA).
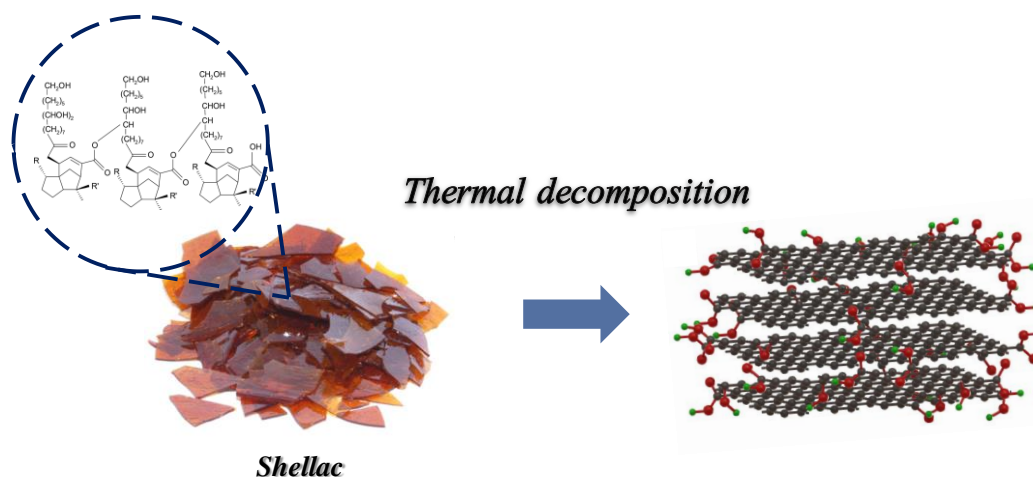
Figure 5. Thermal decomposition of amorphous polymer shellac.

In addition to the method of enhancing the thermal conductivity of amorphous polymers by changing chain conformation, there is also a study to increase the crystallinity of polymers. Generally, the amorphous polymers have relatively low thermal conductivity due to the random chain conformation which reduces the phonon mean free path and results on phonon scattering,[26, 27] while the crystalline polymer shows high thermal conductivity. Shellac, a natural low-cost biopolymer, has been extensively used in organic bio-medical devices, pharmaceutical applications due to its biocompatibility with the human body. In addition, its long aliphatic backbone and lower thermal decomposition temperature enable the direct conversion of shellac to TRGO[28]. The amorphous polymer shellac gets TRGO structure by thermal decomposition, and as increasing thermal decomposition temperature, the crystallinity of polymer increases and enhancing thermal conductivity.

Here, we investigated the effects of crystallinity on thermal conductivity by experimental results.

We annealed the shellac film ranging from 100- 900℃ by tube furnace to thermal reduction and investigated the resulting thermal conductivity change. Thermally reduced shellac film at 900℃ shows a significant increase in cross-plane thermal conductivity as high as 1.22 W/m·K, which is six times higher than nature polymer. Additionally, the structural characterization was measured x-ray diffraction (XRD) and Raman spectroscopy and revealing the correlation with cross-plane thermal conductivity.

II. Experimental Method

2.1. Thermal conductivity measurement (Differential 3-omega method)

2.1.1 Theory of 3-omega method
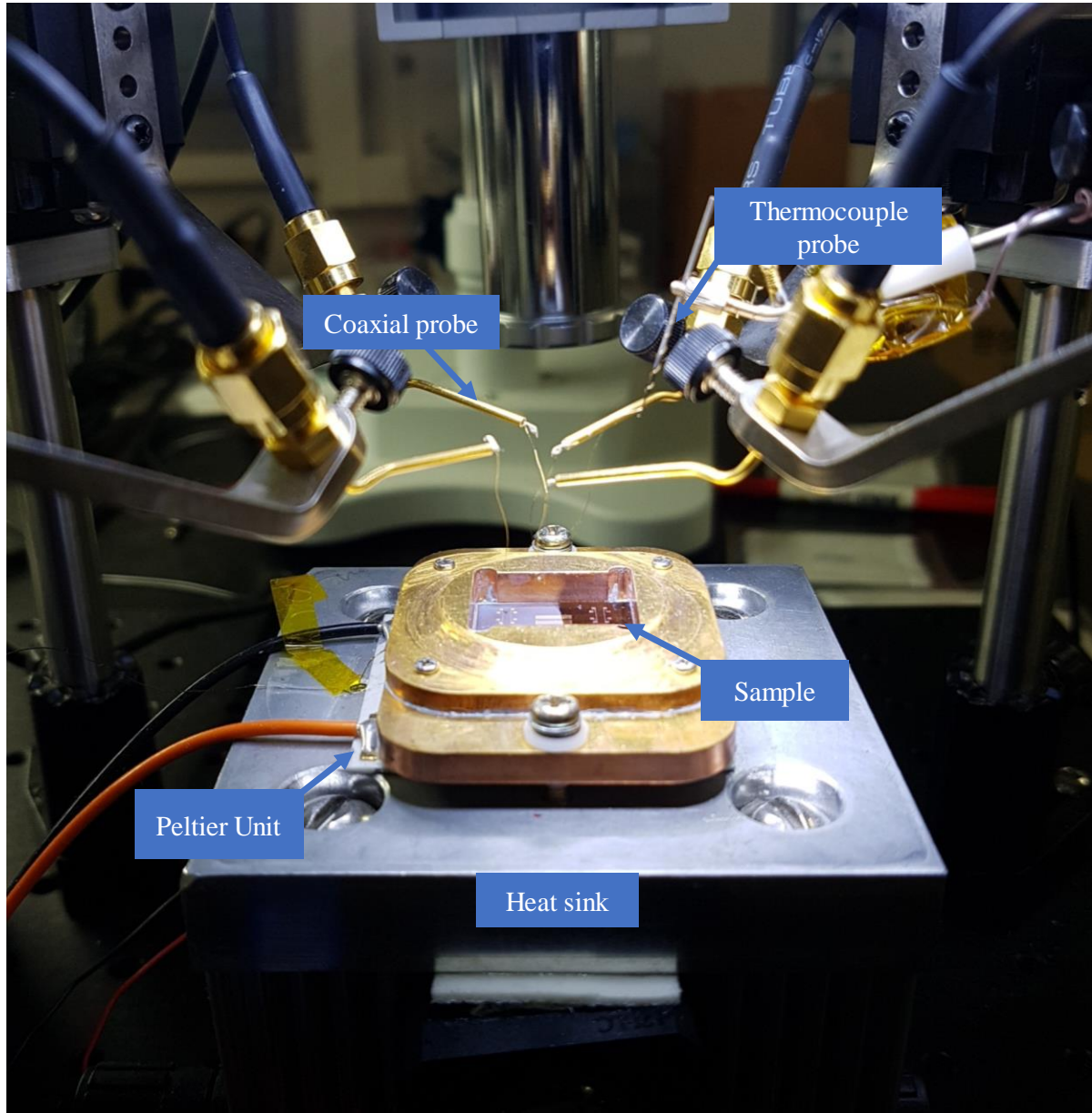
Figure 6. Differential 3-omega method setup.
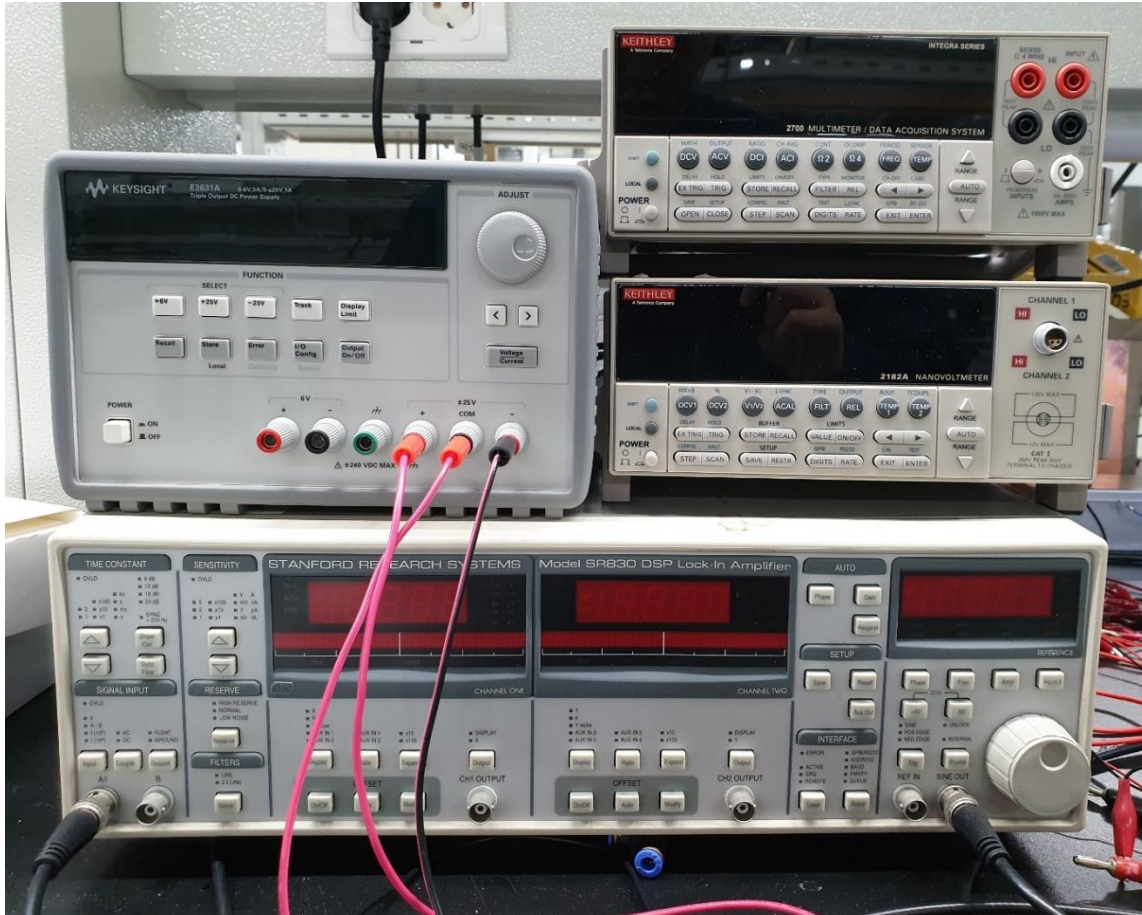
Figure 7. Experimental apparatus used in a differential 3-omega setup.

(Power supply, Lock-in Amplifier, Multimeter).
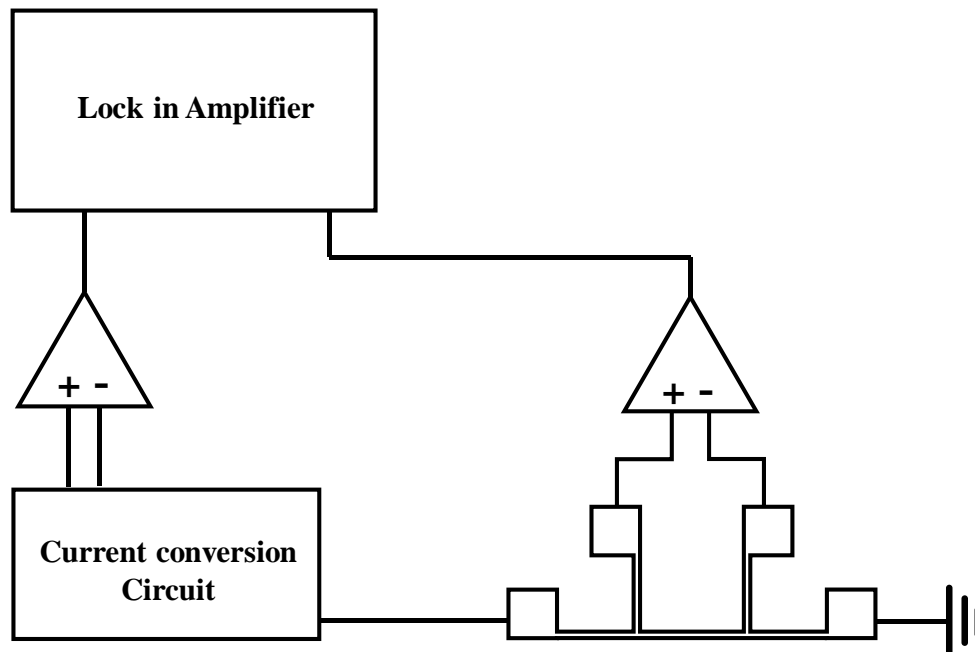
Figure 8. Schematic of a differential 3-omega method.
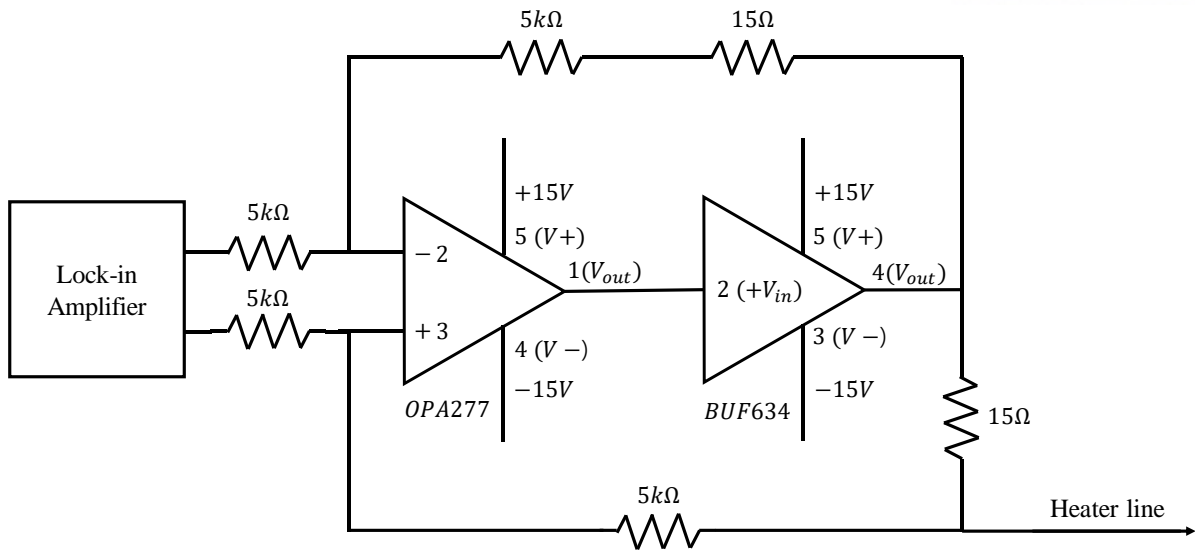
Figure 9. Schematic of voltage to current converter circuit.
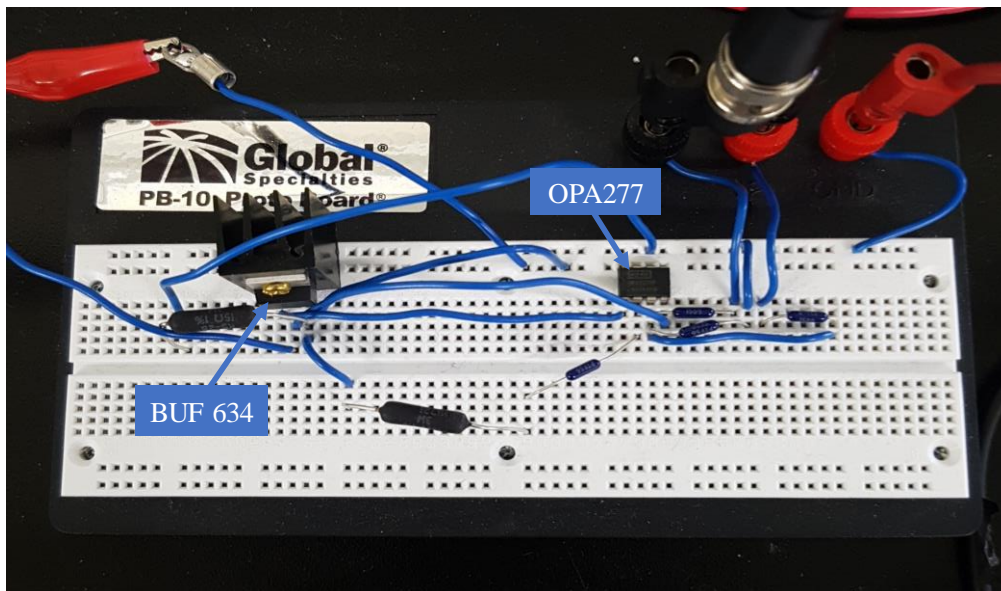
Figure 10. Picture of voltage to the current converter circuit.

Prior to do this research, a precise thermal conductivity measurement setup for thin film is essential. We made the 3-omega method setup which is highly accurate cross-plane thermal conductivity measurement for polymer thin films. This measurement is a transient technique which using electrical signals, so that measuring time is faster than other methods. In this method, a micro-fabricated metal line is deposited on the specimen surface to act simultaneously as a heating source and thermometer detector.

An alternating current (AC) at the first harmonic with frequency of ω generated from lock-in amplifier passing through the heater line over the sample.

$$I_{h,0}(t) = I_{h,0}\,cos(\omega t) \tag{1}$$

This harmonic current generates the Joule heating and generates the temperature change (ΔT_{AC}) in the heater line and the underneath substrate.

$$P_{AC}(t) = \frac{1}{2}I_{h,0}^2 R_{h,0}\,cos(2\omega t) = P_0\,cos(2\omega t) \tag{2}$$

The periodic heating creates a thermal wave that penetrates through the surrounding environment. It occurs temperature oscillation of the heater line which causes the resistance of the heater line to oscillate at 2ω.

$$R = R_0(1 + \beta_h \Delta T) \tag{3}$$

$$\beta_h = \frac{1}{R_0}\frac{dR}{dT} \tag{4}$$

Where, β_h is the temperature coefficient of resistance (TCR) for the heater line.

The third harmonic voltage signal is provided by the ω current modulation and 2ω change in the heater line resistance. The third harmonic voltage can be measured by a lock-in amplifier. The rise in temperature through the cross-planes direction is proportional to the change of third harmonic voltage on the heater line.

$$V_{h,3w} = \frac{1}{2}V_{h,0}\beta_h \Delta T_{AC}, \qquad \Delta T_{AC} = \frac{2V_{3\omega}}{V_{1\omega}\beta_h} \tag{5}$$

Where, $V_{1\omega}$ is given first harmonic voltage from lock-in amplifier and $V_{3\omega}$ is a measured third harmonic voltage.

The temperature rise in the sample (ΔT_s) and reference region (ΔT_r) are extracted by measuring the first and third harmonic voltage between inner pads (interesting part), using a lock-in amplifier (SR830 Lock-in Amplifier, Stanford Research Systems). By subtraction between temperature rise in sample and reference region, we calculate the temperature rise across the thin film (ΔT_f).

$$\kappa = \frac{P_h L}{A\Delta T_f} = \frac{P_h t_f}{w_h l_h\,\Delta T_f} \tag{6}$$

Where P_h demonstrates Joule heating power generated by the heater line, t_f represents the thickness of polymer film and w_h, l_h are the width and length of the heater line, respectively.

9

From the Equation 6, we can derive cross-plane thermal conductivity of the polymer film, by measured first and third harmonic voltage, resistance, and information of heater line across the inner pads.

1-dimensional heat transfer model based on Fourier's law is used to calculate the cross-plane thermal conductivity of the polymer. This model is satisfied because the width of the heater line (50μm) is much larger than the thickness of polymer film (0.15μm ~ 1.8μm). The heater lines were deposited using 5 nm adhesion layer (Cr) and 300 nm of heater line material (Ag) in the e-beam evaporator on the polymer film. The geometry of the heater lines was precisely controlled by using a shadow mask for deposition.

For the deposited polymer film, the thermal excitation frequency range was selected to fulfill the line source approximation appropriate in this heat transfer model. To satisfy the 1D heat diffusion model, the thermal penetration depth should much bigger than half of the width of the heater line (w/2 = 25.25 μm) which can be calculated by the following equation:

$$r = \sqrt{\frac{D}{4\pi f}} \tag{7}$$

Where r represents the thermal penetration depth and D represents thermal diffusivity of the silicon substrate (Silicon: 80 mm^2/s, silicon dioxide: 0.83 mm^2/s).

From the above equation, the lower and upper bound of thermal penetration depth was observed to be 75.36 μm for 1121 Hz and 195.25 μm for 167 Hz for the silicon and 7.68 μm for 1121 Hz and 19.89 μm for 167 Hz for silicon dioxide. Meanwhile, upper bound of thermal penetration depth is much smaller than the substrate thickness (675 μm), which satisfies the 1-dimensional heat transfer model.

2.1.2 Measurement setup

The differential 3-omega setup consists of a probe station (Figure 6), customized voltage to the current convertor circuit, lock-in amplifier, ±15V DC power supply, multimeter, and temperature controller. Figure 8 is a schematic of the differential 3-omega setup. Lock-in amplifier generates the harmonic voltage signal and flow to the voltage to current converter, then flow the alternating current to the heater line. Figure 9 shows illustration of the circuit of voltage to the current converter. Simply voltage to current converter is performed by voltage source supply a voltage as an input to a resistor. In addition, we added an operational amplifier and buffer amplifier to make single-ended output and act as a voltage follower which isolates the output circuit, so the input is not affected in any way by the output device. Then, the lock-in amplifier detects and measures the first harmonic and third harmonic voltage signal between inner pads of the heater line.

Lock-in amplifier (SR830) can generate the desired waveform then, detect and measure a very small AC signal with the reference frequency and phase. The signal generated by the lock-in amplifier flows through the sign out to the circuit and heater line, then generated 3-omega voltage signal between inner pads flows into the sign-in and interpreted. 3-omega voltage is very small in the range of microvolt, so amplifying is required for measurement. Lock-in amplifiers use phase-sensitive detection (PSD) technique to separate the input signal components from noise signals. The Lock-in amplifier generates a sinusoidal signal internally, then the experiment is excited by this signal. This input signal is multiplied by a pure signal with the same frequency with the input signal, then results in the DC output signal. In addition, to attenuate noise by using a low pass filter to narrow the bandwidth of the input signal.

The differential 3-omega method is divided into two steps. Fist, the sample region (film + substrate) temperature rise is derived from the ratio of measured V_{3w} and V_{1w}, and second, the temperature rise on reference region, then the temperature rise on film is derived by subtraction between ΔT_s and ΔT_r.

Precise information about the heater line width, length, temperature coefficient of resistance, and thickness of the film is needed to calculate the cross-plane thermal conductivity of polymer thin film. V_{3w} and V_{1w} signals are precisely measured using a lock-in amplifier (Stanford Research, SR830). The Lock-in amplifier is acting simultaneously as a function generator and a signal detector. This instrument generates an AC signal at ω and flew away through the outside pad of the heater line, then collect the phase-locked voltage at ω and 3ω between inner pads.

The geometry of the metal line is precisely controlled by using a fabricated shadow mask. The heater line patterned on the shadow mask has 50μm width and 2.65mm length between inner pads. By an optical microscope, width of thirty heater lines are measured and a standard deviation was calculated to 0.915% (Average heater line width = 50.45 μm).
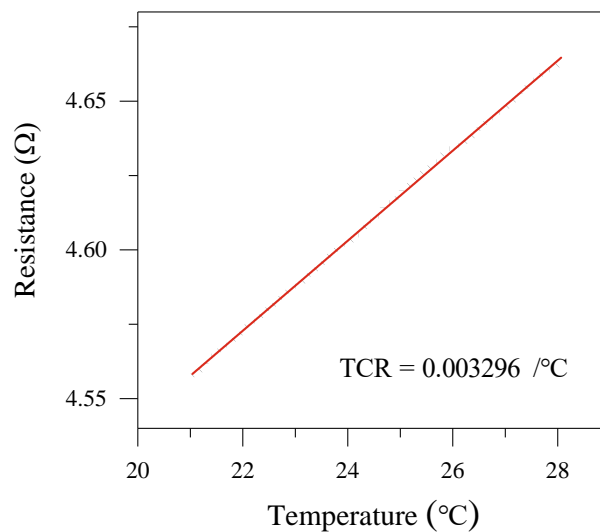
Figure 11. Temperature coefficient of resistance of the heater line.

The heater line's the temperature coefficient of resistance is calculated by the ratio of resistance change during the temperature difference. The heater line is deposited 5 nm adhesion layer (Cr) and 300 nm of heater line material (Ag) by using an e-beam evaporator on the polymer film. The temperature controller (Newport, model 3700) using the Peltier module was used to increase the temperature of the set-up environment. The temperature and resistance changes of the heater line were measured using a multimeter at the same time as slowly raising the temperature of the setup from 20℃ to 30℃. Temperature coefficient of resistance (β_h) of the heater line is calculated by the following equation.
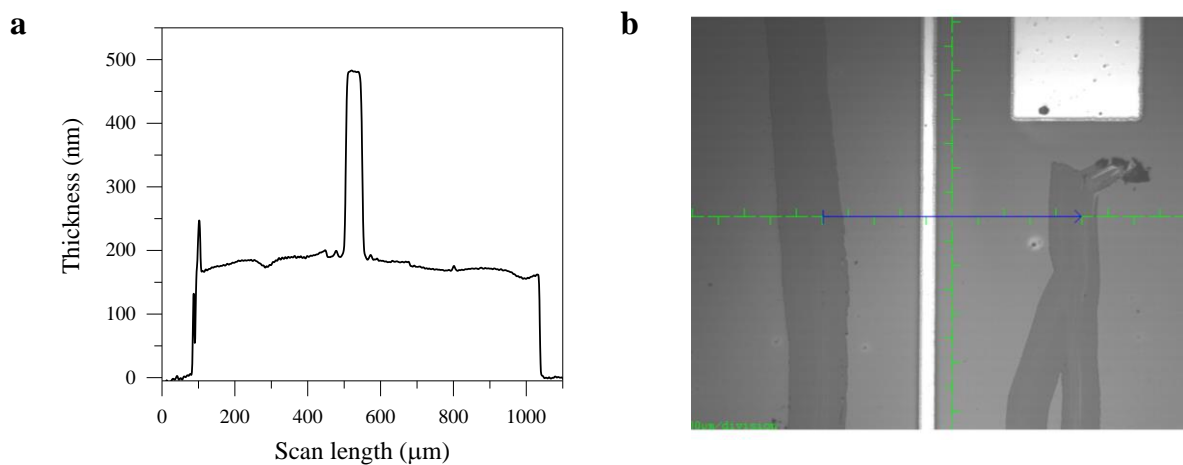
Figure 12. (a) Sample thickness of nearby the heater line was measured by the surface profiler. (b) The optical view of the sample.

The thickness of the polymer film was measured by surface profiler (KLA Tencor, P6). To reduce errors, a reference point was created by scratching the sides of the heater line with a doctor blade to measure the film thickness right next to the heater line. As shown in figure 12(b), the scratch completely removed to the substrate and doctor blade doesn't left any scratches on SiO_2 wafer surface. The film thickness was measured at four different locations (near to each heater line) to validate the uniformity of the polymer film and yielded a standard deviation (σ_t) of 1.32%. The thickness of each heater line was also measured simultaneously. The roughness value (R_a) of the polymer surface was calculated using the line profile (Figure 12a) and the measured roughness was found to be much smaller than the film thickness (less than 3.05%)

2.2 FT-IR spectroscopy

FT-IR spectra were measured on a Varian 670 spectrometer which uses a specular reflectance accessory at a grazing angle of 45°. 512 scans were recorded for each sample. Peak analysis is operated by Gaussian function and 2 peaks were used to fitting the spectra of PMAA and PAA data. The

asymmetric carboxylate ($-COO^-$) stretching band (1500-1620 cm^{-1}, peak 1 and 2 of deconvoluted peaks; see Figure 19) and the carbonyl ($-C=O$) stretching band (1640-1760 cm^{-1}, peak 3 and 4 of deconvoluted peaks; see Figure 19) of the carboxyl groups ($-COOH$) were used for peak analysis[19]. Films at pH 1 and 4, carboxyl group bands are dominant which refers to less degree of ionization. As the degree of ionization increased further, carboxylate bands became dominant. The degree of ionization was calculated by the proportion of peak area.

$$\alpha = \frac{A_{COO^-}}{A_{COO^-} + A_{COOH}} \times 100\% = \frac{(A_{peak\,1} + A_{peak\,2})}{(A_{peak\,1} + A_{peak\,2}) + (A_{peak\,3} + A_{peak\,4})} \times 100\% \quad (8)$$

2.3 Elastic modulus measurement

Elastic modulus measurement was measured with Veeco Multimode Atomic force microscopy which was equipped with a silicon contact mode atomic force microscopy (AFM) probe. Ahead of measurement, the contact mode probe was calibrated against a SiO_2 wafer of known elastic modulus. Samples were attached on the instrument stage by double-sided tape to reduce sample drift during measurement. Elastic Modulus of polymer films was measured by calculation of average value on 9 different points. The elastic modulus of the polymer film was calculated from the F-D curve. Silicon AFM tip is a pyramidal shape, the radius of curvature is 6 nm and cantilever spring constant is 0.29 N/m. We note that the elastic modulus of reference material SiO_2 was measured 60 GPa. For reference check, commercial polymer elastic modulus was measured by AFM measurement, and the measured values (polymethyl methacrylate: 2.29 GPa, polystyrene: 3.16 GPa) were found to be consistent with reported values.[29, 30]

2.4 Viscosity measurement

Viscosity was measured on a rheometer (Thermoelectron, Haake MARS III - ORM Package) using a steel circular plate with a 35 mm diameter. The sample solution's concentration is fixed to 0.5 wt %. For viscosity measurement, the measurement was done at a gradually increasing shear rate from 1 to 200 s^{-1}. We take 3 different points (120 s^{-1}, 150 s^{-1}, 200 s^{-1}) from whole data.

2.5 ^{13}C NMR Measurement

The tacticities of PMAAs were analyzed using a ^{13}C NMR spectrometer (Bruker, AVANCE III HD (400 MHz)) with CDCl$_3$ as the solvent after methylation, while the tacticity of PAAs was analyzed using a ^{13}C NMR spectrometer (Varian, VNMRS 600 (600 MHz)) with D$_2$O as the solvent and the pH was controlled to 12 by adding 1 M NaOH solution in D$_2$O[31].

III. Sample preparation

3.1 Synthesis of polymer

3.1.1. Synthesis of s-PMAA[32]

Firstly, to a suspension of sodium methacrylate (4.43 g, 41.0 mmol) in anhydrous THF (13.0 ml) in the presence of 2,6-di-tert-butyl-p-cresol (6.51 mg, 0.030 mmol), solution of tert-butyldimethylchlorosilane (4.00 g, 27.1 mmol) in anhydrous THF (10.0 ml) was added dropwise in an ice bath under a nitrogen atmosphere. Then the solution was stirred at ambient temperature for 30 h. After evaporating solvent, the reaction mixture was washed with n-hexane and filtrated. To purify the crude product, the alumina column was used. The product was obtained as a colorless liquid.

A polymerization of TBDMSMA was carried out as follows in the glove box. A 50 ml glass vial equipped with a stirring bar was charged with TBDMSMA (2.00 ml, 8.70 mmol), AIBN (0.043 mmol) and anhydrous toluene (3.60 ml) as a solvent. The vial was capped with a rubber septum and sealed with parafilm and bubbled with argon for 30 min. Then the polymerization was carried out at 80 °C for 24 h. To isolate the polymer, the reaction mixture was precipitated by using methanol (75.0 ml). Finally, the precipitation was filtrated and dried under reduced pressure.

Hydrolysis of poly(TBDMSMA) was carried out after obtaining dried poly(TBDMSMA). To a suspension of poly(TBDMSMA) (432 mg) in methanol (40.0 ml), hydrochloric acid (11.0 M, 2.00 ml) was added and refluxed for 24 h. After evaporating solvent, the reaction mixture was washed with diethyl ether and filtrated. The product was dried under reduced pressure.

Finally, methylation of s-PMAA was carried out after obtaining dried s-PMAA[33]. To a solution of s-PMAA (100 mg) in THF/H_2O mixture (20 ml, 1:1 v/v), (trimethylsilyl)diazomethane solution was added dropwise. The formation of nitrogen bubbles and decoloration has occurred and (trimethylsilyl)diazomethane solution was added until there are no nitrogen bubbles and decoloration. The solution was stirred at ambient temperature for 6 h. After evaporating solvent, the product was dried under reduced pressure and dissolved in $CDCl_3$ for NMR analysis.

3.1.2. Synthesis of a-PMAA [1]

Firstly, to a suspension of sodium methacrylate (1.75 g, 16.2 mmol) in anhydrous THF (5.00 ml) in the presence of 2,6-di-tert-butyl-p-cresol (2.58 mg, 0.012 mmol), solution of triisopropylsilyl chloride (2.00 g, 10.7 mmol) in anhydrous THF (4.30 ml) was added dropwise in an ice bath under a nitrogen atmosphere. Then the solution was stirred at ambient temperature for 25 h. After evaporating solvent, the reaction mixture was washed with n-hexane and filtrated. To purify the crude product, the alumina column was used. The product was obtained as a colorless liquid.

A polymerization of TIPSMA was carried out as follows in the glove box. A 50 ml glass vial equipped with a stirring bar was charged with TIPSMA (2.00 ml, 7.44 mmol), AIBN (0.037 mmol), and

anhydrous toluene (5.80 ml) as a solvent. The vial was capped with a rubber septum and sealed with parafilm and bubbled with argon for 30 min. Then the polymerization was carried out at 80 ℃ for 14 h. To isolate the polymer, the reaction mixture was precipitated by using methanol (75.0 ml). Finally, the precipitation was filtrated and dried under reduced pressure.

Hydrolysis of poly(TIPSMA) was carried out after obtaining dried poly(TIPSMA). To a suspension of poly(TBDMSMA) (216 mg) in methanol (20.0 ml), hydrochloric acid (11.0 M, 1.00 ml) was added and refluxed for 96 h. After evaporating solvent, the reaction mixture was washed with diethyl ether and filtrated. The product was dried under reduced pressure.

Finally, Methylation of a-PMAA was carried out after obtaining dried a-PMAA. To a solution of a-PMAA (100 mg) in THF/H_2O mixture (20 ml, 1:1 v/v), (trimethylsilyl)diazomethane solution was added dropwise. The formation of nitrogen bubbles and decoloration has occurred and (trimethylsilyl)diazomethane solution was added until there are no nitrogen bubbles and decoloration. The solution was stirred at ambient temperature for 6 h. After evaporating solvent, the product was dried under reduced pressure and dissolved in $CDCl_3$ for NMR analysis.

3.2. Tacticity analysis

To characterize the tacticity of synthesized and bought polymers, ^{13}C NMR spectrometer was used to analyze. By calculating the ratio of a syndiotactic triad, heterotactic triad, and isotactic triad polymer tacticity is characterized.
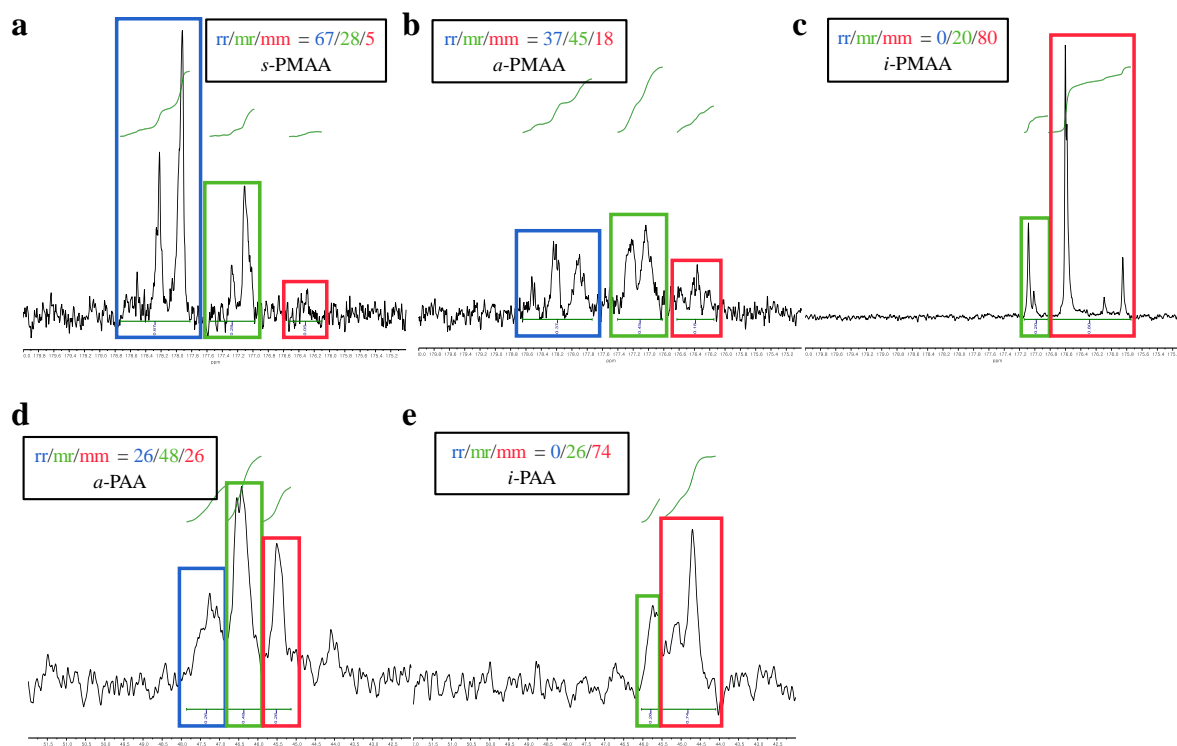

Figure 13. ^{13}C NMR spectrum of polymers.

Polymer	Major Tacticity	Triad ratio (rr/mr/mm)	M_n (Da)	Vendor
PMAA	Syndiotactic	**67**/28/5	13,000	Synthesized[a]
	Atactic	37/**45**/18	3,600	Synthesized[a]
	Isotactic	0/20/**80**	28,000	Polymer Source
PAA	Atactic	26/**48**/26	100,000[b]	Sigma Aldrich
	Isotactic	0/26/**74**	49,000	Polymer Source

a. For detailed procedures, see supplementary methods; section A-2 and A-3. b. M_w value.

Table 1. Overall information about polymers used in this work.

3.3 Polymer film fabrication

3.3.1. Polymer Solution Preparation

First, for PMAA samples, the required amount of polymer was dissolved in DI water by heating at 80°C to ensure complete dissolution. The polymer solutions were then allowed to cool down to room temperature and the pH was adjusting by adding 1 M hydrochloric acid (HCl) or 1 M sodium hydroxide (NaOH) solution. Finally, the final concentration of the solution was adjusted to 1 wt % by adding DI water. Mixture DI water and ethyl alcohol (1:1 v/v) were used as a solvent for a-PAA and i-PAA.

3.3.2. Thin Film Preparation

Figure 14. Schematic of polymer thin film fabrication.
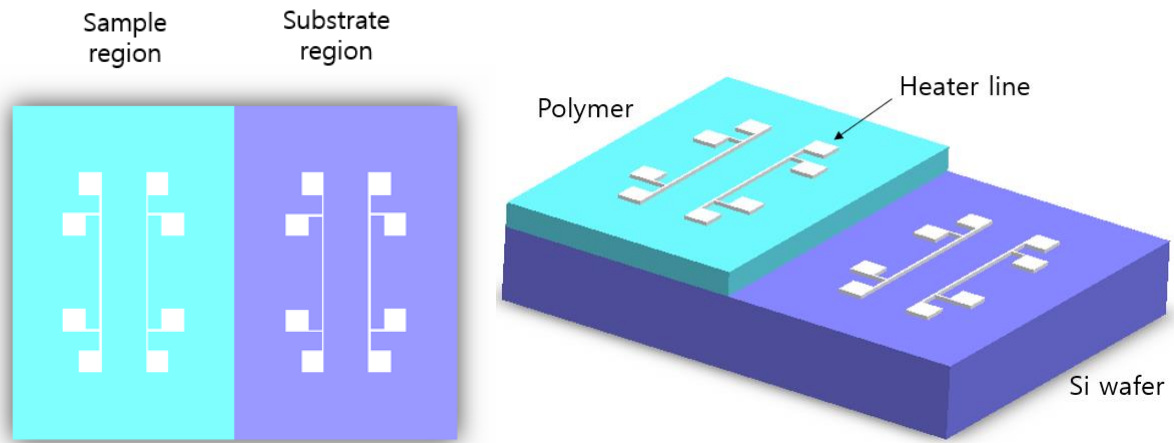
Figure 15. Illustration of differential 3-omega method sample.

Silicon wafers were cut in 15 mm × 20 mm size using dicing saw. Obtained wafers were cleaned by washing process by sonicating for 5 minutes in each step using DI water, acetone, and isopropyl alcohol. Then, the surface of the silicon wafer treated with O_2 plasma treatment for 3 min at 100 W power. The prepared 1wt% solutions were coated by spin coating on completely cleaned silicon wafer substrate at 300 rpm for 1 hour (Low rotation speed spin-cast). This low rpm led to a slow drying of polymer solution (60 minutes), which is expected to reduce the anisotropy in the polymer film, as well as large film thickness (0.15 - 1.8 μm) which enhances the accuracy of the differential 3-omega measurement. After spin coating, the sample was annealed at 100℃ for 30 minutes to evaporate the remaining solvents. Prepared samples are used for thermal conductivity measurement, Fourier transforms infrared (FT-IR) spectroscopy and elastic modulus measurement.

For differential 3-omega method, half part of the sample was scratched out carefully by a steel blade, and clearly removing remain polymer over wafer by wiping with a cotton swab soaked in DI water and acetone each. Silver heater lines were deposited by the e-beam evaporator.

3.4 Thermal annealing of shellac film preparation
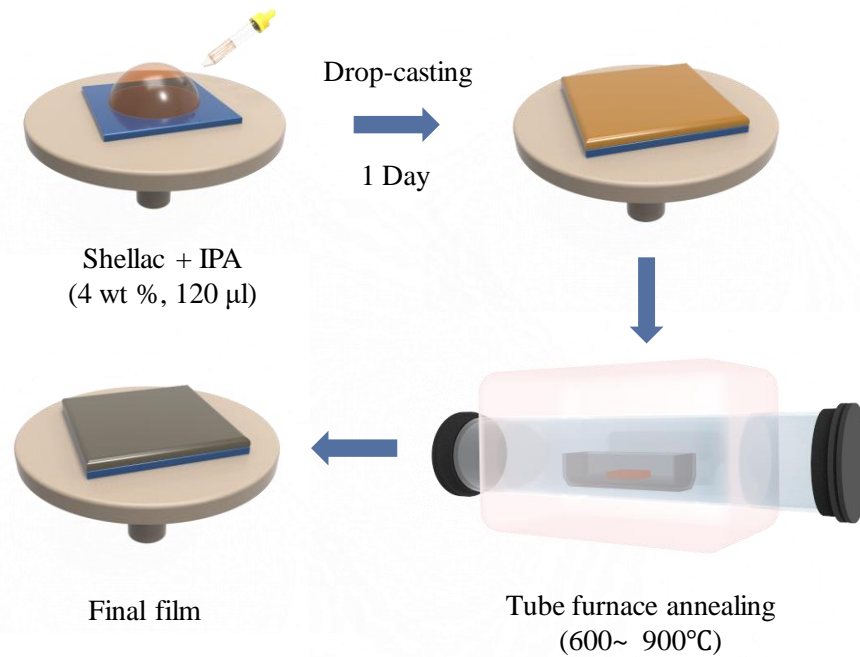
Figure 16. TRGO film preparation procedure.

In a typical modification process, 4 mg of shellac polymer (MW, 1006) was dissolved in 10 ml isopropanol. The solution is kept for 20 minutes on a hot plate, maintained at 60℃, to an obtained homogeneous solution. Polymer solutions (120 ul) were coated by drop casting on cleaned silicon wafers with 100 nm SiO_2 layer, and the resulting films were left for air drying for 1 hour. The prepared drop-casted film is thermally annealed at a targeted temperature with a tube furnace for 30 minutes.

For thermal conductivity measurement sample, a half part of the drop-cast film was removed by using a steel blade, and the cleared area was further cleaned by a cotton swab dipped in water and ethanol to give a clean polymer-free reference region. The film was then annealed at several temperatures, ranging from 100- 900℃, to modulate the film properties. To electrically isolate the heater line from the conductive film, the 100nm Al_2O_3 layer was deposited by DC sputtering. The heater lines on both sample and reference regions were deposited by E-beam evaporation deposition (5 nm Cr + 300 nm Ag) with an elaborately manufactured shadow mask.

IV. Results and discussion

4.1. Validation of the differential 3-omega method results.

To validate the accuracy of the thermal conductivity measurement, we measured three known polymers (PMAA, PS, PSS).

Firstly, we measured the resistance between the inner pad by multimeter with 4-point probe measurement. Then, determine the amount of first harmonic voltage applied to the inner pad of the heater line, which generates 0.1W followed by Ohm's Law. Then, measuring the third harmonic voltage at 7 different thermal excitation frequency by the lock-in amplifier. Also, the temperature coefficient of resistance for each heater line is determined separately. Finally, by plotting the overall temperature difference versus thermal excitation frequency. The temperature difference of polymer is derived by subtraction between temperature difference at sample and substrate region.

The following graph shows the temperature difference versus thermal excitation frequencies. The temperature difference between the heater line and the underneath specimen is reduced as the applied frequency is increased. As applying frequency getting higher, the penetration depth is getting low, so that the heat-affected region is getting shorter.
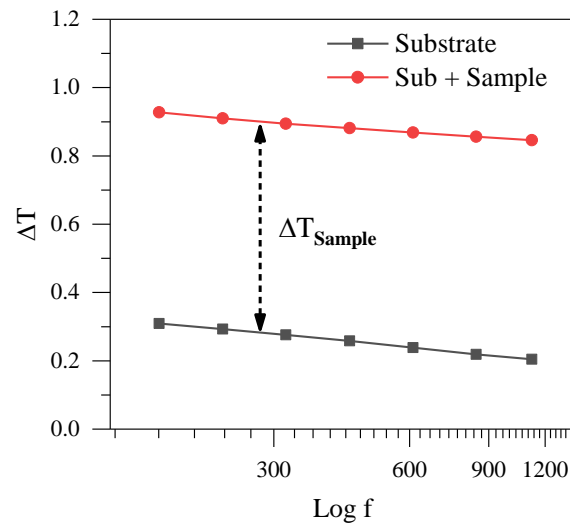
Figure 17. The graph of temperature difference versus thermal excitation frequency for substrate region and sample region.

The cross-plane thermal conductivity is derived by measured TCR, temperature difference of sample, and thickness of thin polymer film. By considering the thermal conductivity equation and substituting all required information, the thermal conductivity of polymethyl methacrylate is derived as 0.22 W/m·K which is correspond with the previous report[34]. Furthermore, the cross-plane thermal conductivity of polystyrene and polystyrene sulfonate is measured by the same procedure, and values are derived by 0.17 W/m·K and 0.39 W/m·K each[34, 35].
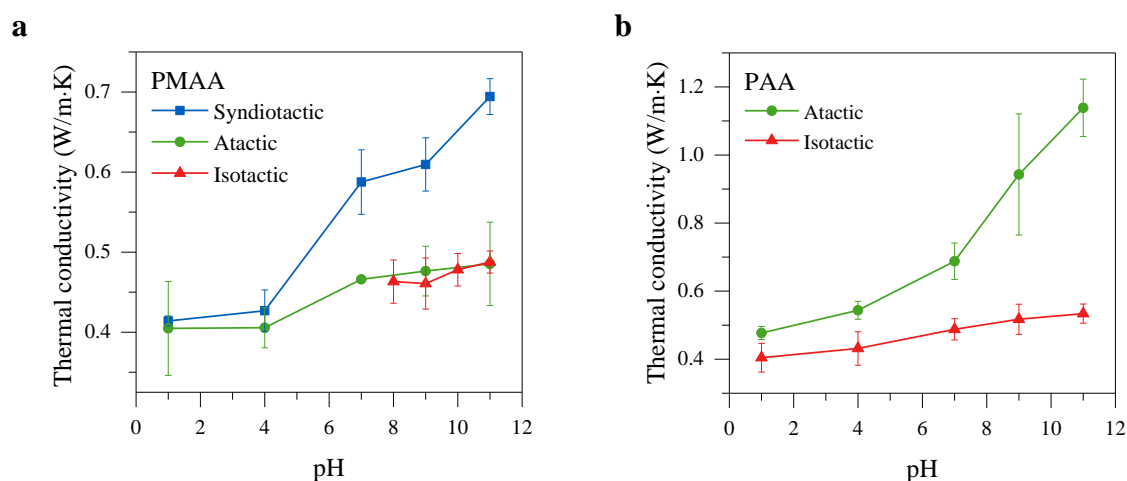
4.2. Tacticity dependent cross-plane thermal conductivity in electrostatically engineered amorphous polymers

4.2.1. Cross-plane thermal conductivity of PMAA and PAA by different tacticities.

After validating the accuracy of the thermal conductivity measurement setup, we proceed with the thermal characterization of PMAA and PAA by different tacticities with different pH.

Polyacrylic acid (PAA; atactic) is a weak polyelectrolyte which is easy to ionize. This polymer consists of a C-C backbone with a carboxylic acid group. In a water solution, many of the side chains of PAA lose their protons and acquire a negative charge. According to previous studies, as the pH of atactic PAA increases, polymer chain extended by the coulombic repulsive force between ionized carboxylic acid groups, thereby increasing the thermal conductivity of the polymer film.

Furthermore, we conducted this study in anticipation of the effects of thermal conductivity enhancement will be different depending on tacticity difference. We made polymer films of syndiotactic, atactic, isotactic PMAA and atactic, isotactic PAA, and measure cross-plane thermal conductivity by our measurement setup.

Figure 18. The cross-plane thermal conductivity of PMAA and PAA films coated from different pH levels by tacticity dependent.

As shown in figure 18, the thermal conductivity of *s*-PMAA increased from 0.42 ± 0.04 W/m·K to 0.69 ± 0.04 W/m·K as pH increased from 1 to 11. Likewise, the thermal conductivity of *a*-PAA increased from 0.47 ± 0.02 W/m·K to 1.14 ± 0.04 W/m·K as pH increased from 1 to 11. However, in other tacticities, the thermal conductivity enhancement effect was insignificant as ionization increased. We expected this insignificant enhancement in thermal conductivity of *a*-PMAA, *i*-PMAA, and *i*-PAA is caused by steric repulsion among adjacent negative charged pendant groups, which disturb the chain linearization[36].
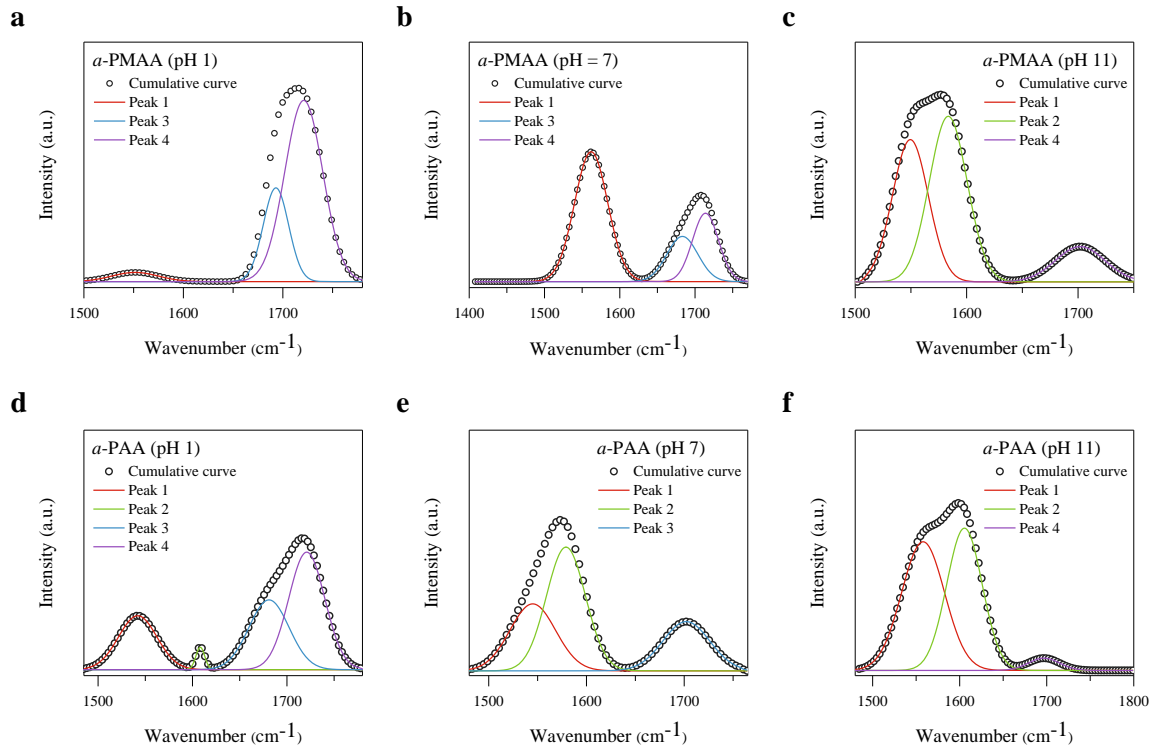
4.2.2 Degree of Ionization

Figure 19. Representative FT-IR spectra for PMAA and PAA with deconvoluted peaks.
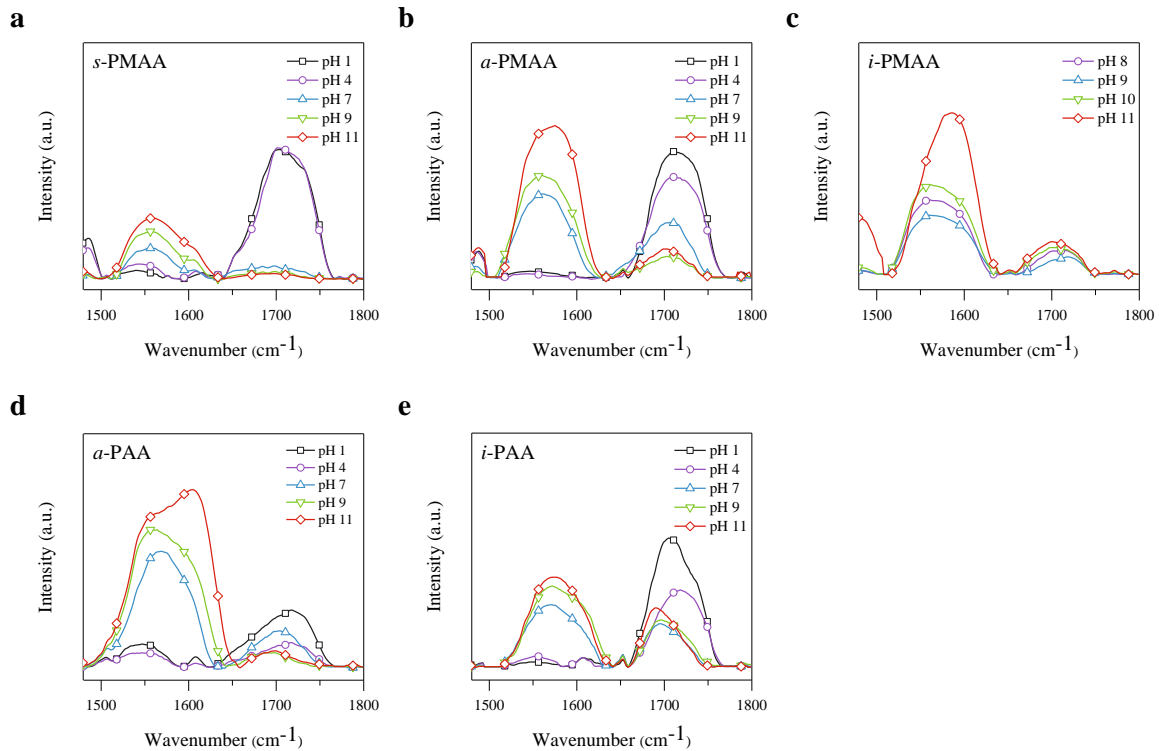

Figure 20. FT-IR spectra analysis.

Fourier transform infrared spectroscopy (FT-IR) was used to quantify the ionization of PMAA and PAA films with different tacticities. Peak analysis is operated by Gaussian function with 2 peaks that were used to fit the PMAA and PAA spectra. Figure 19 is deconvoluted examples of the FT-IR spectra of polymer films. The asymmetric carboxylate (−COO⁻) stretching band (1500-1620 cm⁻¹, peak 1 and 2 of deconvoluted peaks; see Figure 19) and the carbonyl (−C=O) stretching band (1640-1760 cm⁻¹, peak 3 and 4 of deconvoluted peaks; see Figure 19) of the carboxyl groups (−COOH) were used for deconvoluted peaks. Figure 20 shows FT-IR spectra according to pH changes for each tacticity. At higher pH for all tacticities, the area of carboxylate peak is dominant, which means it is more ionized. A lower pH for all tacticities, the area of carboxyl peak is dominant.

a

b
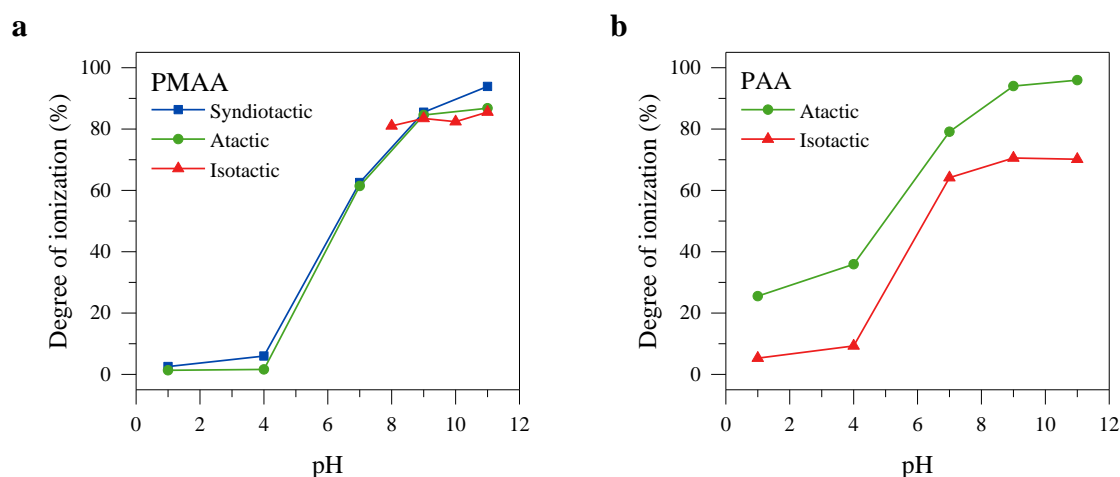
Figure 21. Degree of ionization in PMAA and PAA polymer films with different tacticity.

As shown in figure 21 the polymers were highly ionized at pH 11 regardless of the polymer tacticity, and it means most of the side chains have negative charges. As shown in previous studies, highly ionized *a*-PAA generates the repulsive force between negative charged ionized groups, which results in chain extension and thermal conductivity enhancement. Also, *s*-PMAA showed a similar tendency to increase thermal conductivity as ionization increased. However, the ionization of *a*-PMAA, *i*-PMAA, and *i*-PAA increased with higher pH, but the thermal conductivity enhancement effect was negligible. Therefore, it is assumed that the difference of tacticity, a difference of side-chain arrangement, will take an important role in thermal conductivity enhancement.

4.2.3. Elastic modulus and viscosity

Furthermore, we measured elastic modulus and viscosity of polymer to investigate the correlation between the measured thermal conductivity and chain extension which is induced by ionization. Elastic modulus of polymer films was measured by Atomic force microscopy. The viscosity of the polymer solution was measured by the rheometer.

22
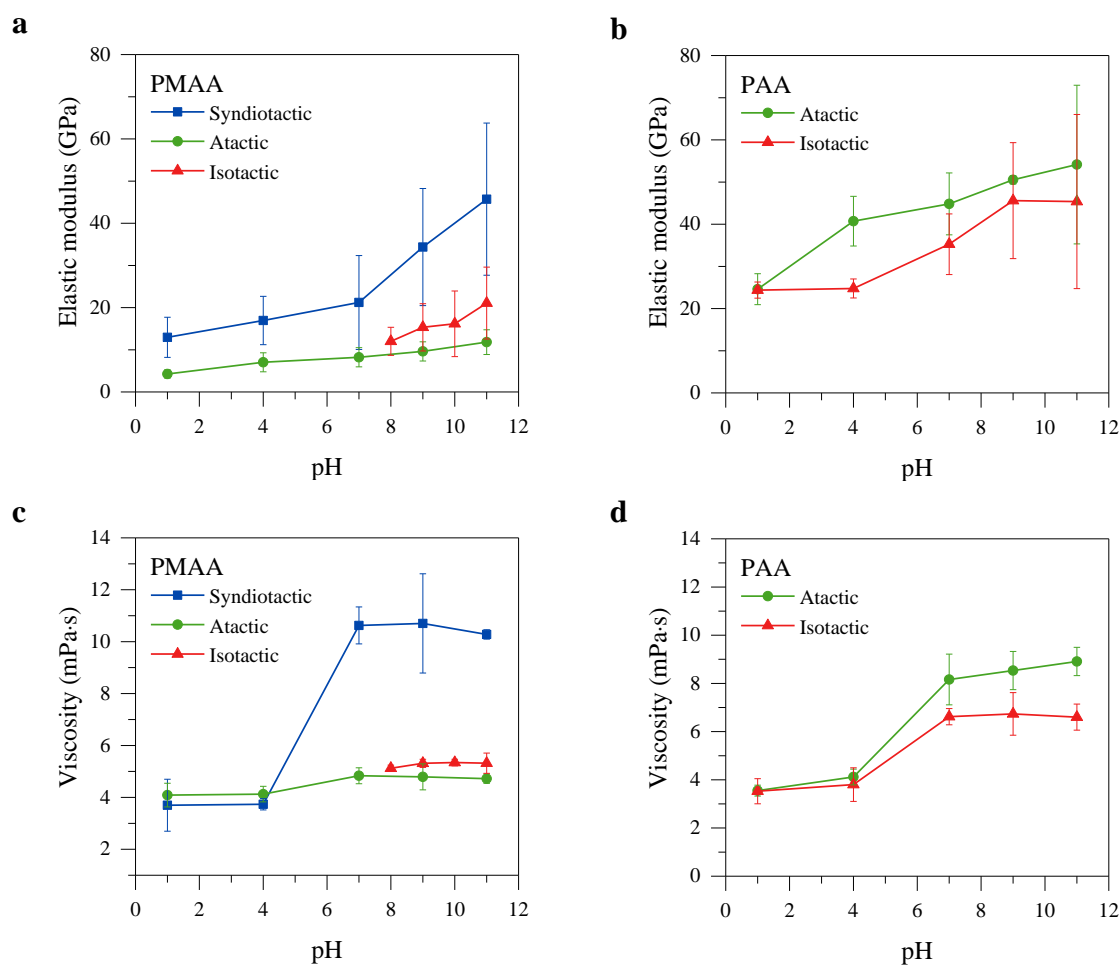
Figure 22. Elastic modulus and viscosity of PMAA and PAA films coated from polymer solutions of different pH levels by tacticity dependent.

As shown in figure 22a, s-PMAA shows an increase in elastic modulus as pH increased, such as thermal conductivity tendency. However, in *a*-PMAA and *i*-PMAA, there was a negligible enhancement of the elastic modulus as polymer ionization increased. PMAA has a relatively large methyl group, which causes a steric hindrance that affects the conformation of the polymer chain. The steric hindrance by a methyl group and the electrostatic repulsion between ionized side chains compete and affect the chain extension of the polymer chain conformation[37]. In *s*-PMAA, the effect of the interfering chain extension is minimized. Because the alternating spatial arrangement of carboxylates and methyl groups of syndiotactic polymer counterbalance the effect of interference. As a result of this conformation, elastic modulus and thermal conductivity show large enhancement at higher pH. In *a*-PMAA and *i*-PMAA, these obstruct effects were dominant, resulting in a negligible increment in elastic modulus.

On the other hand, PAA does not have a large methyl group among the main chain. Therefore, repulsive force among carboxylates has a dominant influence on chain conformation. In other words, regardless of the spatial arrangement of carboxylate, has a repulsive force that can easily rotate the polymer main chain, affects the extension of chain conformation[36]. As a result, the enhancement of

23

elastic modulus for *a*-PAA and *i*-PAA was considerable. However, despite the chain extension proved by elastic modulus on both tacticities, thermal conductivity enhancement of *i*-PAA is negligible. We assume that the inconsistency between elastic modulus and thermal conductivity of *i*-PAA generate from the relatively large torsion among the *i*-PAA polymer chain inhibits the heat propagation, therefore reduce the enhancement of thermal conductivity.

4.3. Thermal annealed shellac thermal conductivity
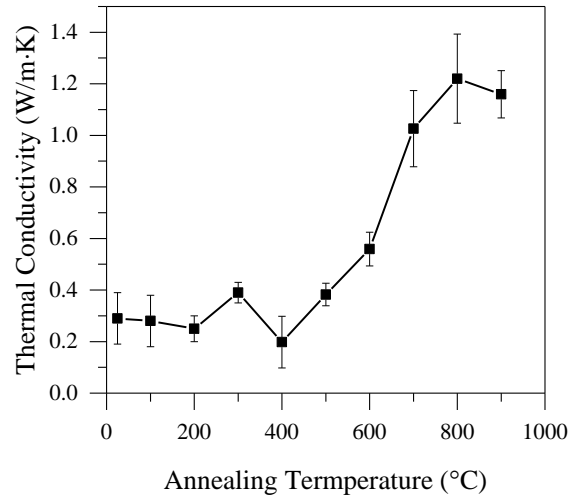
Figure 23. Cross-plane thermal conductivity of annealed shellac film.

The constituent polymer shellac displays very low thermal conductivity (0.3 $Wm^{-1}K^{-1}$), similar to other amorphous polymers[18]. The cross-plane thermal conductivity is almost constant till the sample underwent thermal reduced temperature at 500°C. However, as the thermal reduction temperature has been increased to 600°C, the formation of graphene oxide has been observed and the thermal conductivity increases to 0.6 $Wm^{-1}K^{-1}$. However, as reduction temperature increases, the film displays a thermal conductivity ($k_{max} = 1.22 \pm 0.02$ W/m·K), one order higher than amorphous shellac polymer.
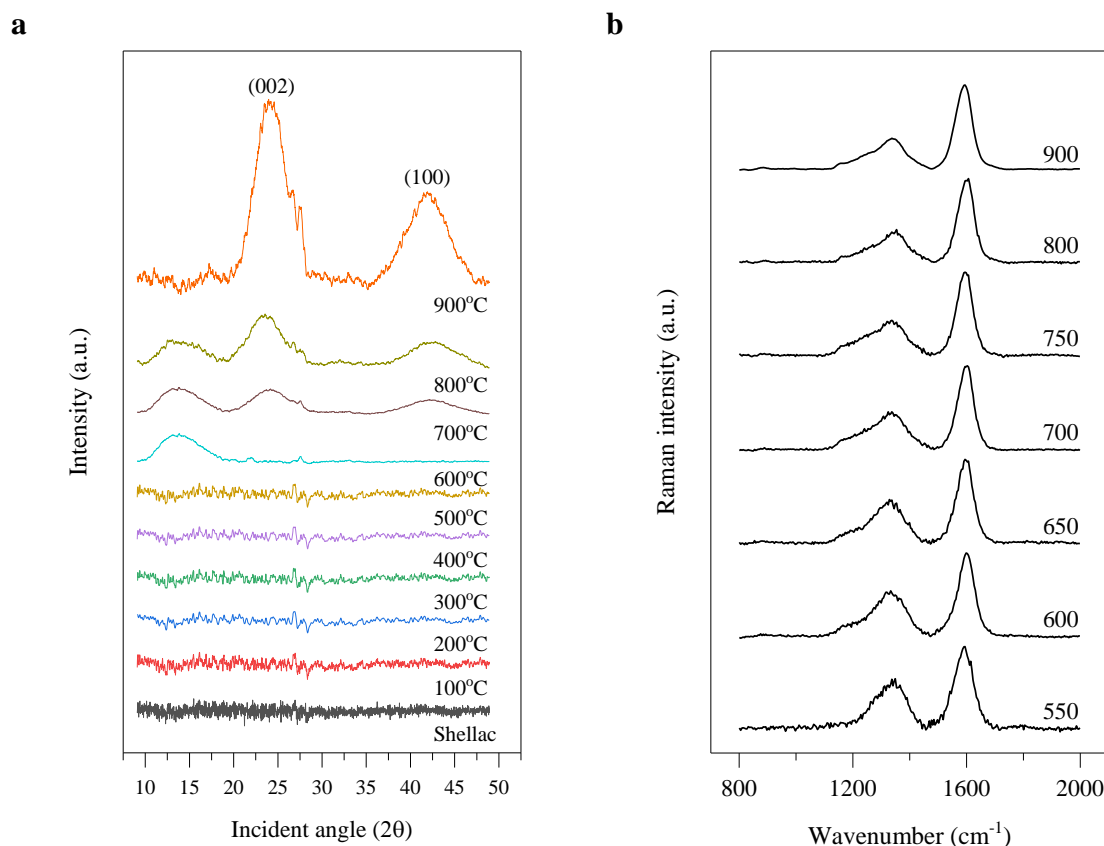
Figure 24. (a) X-ray Diffraction spectra for TRGO films at various temperatures. (b) Raman spectra for TRGO films at various temperatures.

To find out the cause of the cross-plane thermal conductivity increment due to the rise of thermal reduction temperature, we investigate the structural properties of the annealed sample by XRD and Raman spectroscopy. As shown in figure 24 (a), XRD analysis operated for shellac polymers annealed by various temperatures. The polymer doesn't show any peak until annealing temperature arise to 500℃. From 600℃, broadband at 13.9° is observed which represents the formation of graphene oxide. Furthermore, when the thermal reduction gradually increased to 900℃, we observed the intensity of GO peak is reduced and finally it was disappeared at 900℃, and shows the development of reduced graphene oxide peak at 25°. As a result, the higher the annealing temperature above a certain level, the higher the characteristic of RGO.

Raman spectroscopy is operated to confirm the crystallinity of the annealed samples. As shown in figure 24 (b), the peak located at 1350 cm^{-1} (D band) which is related to the disordered structures and the G band centered at 1600 cm^{-1} was observed[38]. The intensity of D and G peaks is used to determine the defects in the structure. At 500℃, I_D/I_G ratio is 1.0. As annealing temperature arises to 900℃, the intensity of the D band decreased, and the G band showed development. Then, the I_D/I_G ratio is

decreased as annealing temperature increases, it refers that the crystallinity of the sample has been increased. From the above analysis, as the thermal reduction temperature increases, the development of RGO and the improvement of crystallinity were observed, which seems to be a factor that the enhancement of the cross-plane thermal conductivity.

V. Conclusion

In this study, we systematically investigated the effect of chain extension and crystallinity in different amorphous polymer's cross-plane thermal conductivity. We used PMAA and PAA with different tacticities (syndiotactic, atactic, isotactic) for studying the effect on polymer film thermal conductivity. The polymer tacticity affects the spatial arrangement of electrostatic repulsion force among the polymer chain, and it affects the polymer chain conformation, elastic modulus, and therefore the thermal conductivity of polymers. In addition, to explore the effect of crystallinity on thermal conductivity, we used the natural biopolymer shellac, which has low thermal decomposition temperature. We systematically investigated the effect of annealing temperature on the cross-plane thermal conductivity of the amorphous natural polymer. All cross-plane thermal conductivity results are measured by the differential 3-omega method setup.

Conclusions of tacticity effects on thermal conductivity in electrostatically engineered amorphous polymers.

- As weak polyelectrolytes ionized, electrostatic repulsive force among adjacent pendant groups stretch the polymer backbone.
- In syndiotactic PMAA, cross-plane thermal conductivity increased to 0.69 ± 0.04 W/m·K at pH 11, as the carboxyl groups of the polymer were ionized which is 1.65 times enhanced from the original polymer. Similarly, the thermal conductivity of atactic PAA increased 1.14 ± 0.04 W/m·K which is 2.42 times enhanced from the original polymer.
- In other tacticities, thermal conductivity enhancement was negligible.
- In all tacticities, the degree of ionization showed high values at high pH, which refers that all polymers were highly ionized (>80%) regardless of polymer tacticity.
- From the elastic modulus and viscosity results of PMAA, steric hindrance by methyl groups and electrostatic repulsion among carboxylates impede chain extension in a-PMAA and i-PMAA. This obstructive effect of methyl groups against the extension is expected to be minimal in s-PMAA due to its alternating arrangement of carboxylates and methyl groups.
- In PAA, since there are no methyl groups to compete with the electrostatic repulsion force, considerable enhancement in elastic modulus and viscosity were observed for both a-PAA and i-PAA. But, the enhanced elastic modulus of i-PAA did not lead to thermal conductivity enhancement.
- From this study, not only chain extension but also torsion of repeat units and steric hindrance should be considered when designing a thermally conductive polymer by extended chain conformation.

<u>Conclusions of crystallinity effect on thermal conductivity in amorphous natural bio-polymer.</u>

- The crystallization on shellac has been begun, when we annealed above at a temperature higher than 600°C.

- As the annealing temperature increases, the cross-plane thermal conductivity of polymer film increases, and thermal reduction of shellac films at temperature 900°C display a substantial increase in cross-plane thermal conductivity ($\hat{k}_{max} = 1.22$ W/m·K), which is six times higher than natural polymer.

- As the annealing temperature increases, I_D/I_G ratio is decreased, which refers that the graphene characteristic increases and the crystallinity of polymer film also increases.

- The enhancement in thermal conductivity in this study has been attributed to heat reduction at high annealing temperature, resulting in the crystallization and having the characteristic of graphene, also reducing inter-layer space which facilitates thermal transport.

VI. Reference

[1]   Novák, P.; Müller, K.; Santhanam, K. S. V.; Haas, O., Electrochemically Active Polymers for Rechargeable Batteries. *Chemical Reviews* **1997,** *97* (1), 207-282.

[2]   Wang, W.; Tang, M.; Zheng, Z.; Chen, S., Alkaline Polymer Membrane-Based Ultrathin, Flexible, and High-Performance Solid-State Zn-Air Battery. *Advanced Energy Materials* **2019,** *9* (14).

[3]   Abbasi, H.; Antunes, M.; Velasco, J. I., Recent advances in carbon-based polymer nanocomposites for electromagnetic interference shielding. *Progress in Materials Science* **2019,** *103*, 319-373.

[4]   Tzong-Lin, W.; Wern-Shiarng, J.; Dai, S. G.; Wood-Hi, C., Effective electromagnetic shielding of plastic packaging in low-cost optical transceiver modules. *Journal of Lightwave Technology* **2003,** *21* (6), 1536-1543.

[5]   Prasher, R., Thermal Interface Materials: Historical Perspective, Status, and Future Directions. *Proceedings of the IEEE* **2006,** *94* (8), 1571-1586.

[6]   Zhu, Y.; Ha, S. Y.; Masel, R. I., High power density direct formic acid fuel cells. *Journal of Power Sources* **2004,** *130* (1-2), 8-14.

[7]   Su, J.; Liu, X.; Charmchi, M.; Sun, H., Experimental and numerical study of anisotropic thermal conductivity of magnetically aligned PDMS/Ni particle composites. *International Journal of Heat and Mass Transfer* **2016,** *97*, 645-652.

[8]   Wang, J.; Xie, H.; Xin, Z.; Li, Y.; Chen, L., Enhancing thermal conductivity of palmitic acid based phase change materials with carbon nanotubes as fillers. *Solar Energy* **2010,** *84* (2), 339-344.

[9]   Dames, C., Ultrahigh thermal conductivity confirmed in boron arsenide. *Science* **2018,** *361* (6402), 549.

[10]   Henry, A.; Chen, G., High thermal conductivity of single polyethylene chains using molecular dynamics simulations. *Phys Rev Lett* **2008,** *101* (23), 235502.

[11]   Shen, S.; Henry, A.; Tong, J.; Zheng, R.; Chen, G., Polyethylene nanofibres with very high thermal conductivities. *Nat Nanotechnol* **2010,** *5* (4), 251-5.

[12]   Roy, A.; Bougher, T. L.; Geng, R.; Ke, Y.; Locklin, J.; Cola, B. A., Thermal Conductance of Poly(3-methylthiophene) Brushes. *ACS Appl Mater Interfaces* **2016,** *8* (38), 25578-85.

[13]   Henry, A., THERMAL TRANSPORT IN POLYMERS. *Annual Rev Heat Transfer Annual Review of Heat Transfer* **2014,** *17* (N/A), 485-520.

[14]   Shen, S.; Henry, A.; Tong, J.; Zheng, R.; Chen, G., Polyethylene Nanofibres with Very High Thermal Conductivities. *Nat. Nanotechnol.* **2010,** *5*, 251.

[15]   Wang, X.; Ho, V.; Segalman, R. A.; Cahill, D. G., Thermal Conductivity of High-Modulus

Polymer Fibers. *Macromolecules* **2013,** *46*, 4937.

[16] Singh, V.;   Bougher, T. L.;   Weathers, A.;   Cai, Y.;   Bi, K.;   Pettes, M. T.;   McMenamin, S. A.;   Lv, W.;   Resler, D. P.;   Gattuso, T. R.;   Altman, D. H.;   Sandhage, K. H.;   Shi, L.; Henry, A.; Cola, B. A., High thermal conductivity of chain-oriented amorphous polythiophene. *Nat Nanotechnol* **2014,** *9* (5), 384-90.

[17] Smith, M. K.;   Singh, V.;   Kalaitzidou, K.; Cola, B. A., Poly(3-hexylthiophene) Nanotube Array Surfaces with Tunable Wetting and Contact Thermal Energy Transport. *ACS Nano* **2015,** *9* (2), 1080-1088.

[18] Kim, G. H.;   Lee, D.;   Shanker, A.;   Shao, L.;   Kwon, M. S.;   Gidley, D.;   Kim, J.; Pipe, K. P., High thermal conductivity in amorphous polymer blends by engineered interchain interactions. *Nat Mater* **2015,** *14* (3), 295-300.

[19] Shanker, A.;   Li, C.;   Kim, G. H.;   Gidley, D.;   Pipe, K. P.; Kim, J., High thermal conductivity in electrostatically engineered amorphous polymers. *Sci Adv* **2017,** *3* (7), e1700342.

[20] Chen, K.;   Harris, K.; Vyazovkin, S., Tacticity as a Factor Contributing to the Thermal Stability of Polystyrene. *Macromolecular Chemistry and Physics* **2007,** *208* (23), 2525-2532.

[21] Glüge, R.;   Altenbach, H.;   Kolesov, I.;   Mahmood, N.;   Beiner, M.; Androsch, R., On the effective elastic properties of isotactic polypropylene. *Polymer* **2019,** *160*, 291-302.

[22] Huang, C.-L.;   Chen, Y.-C.;   Hsiao, T.-J.;   Tsai, J.-C.; Wang, C., Effect of Tacticity on Viscoelastic Properties of Polystyrene. *Macromolecules* **2011,** *44* (15), 6155-6161.

[23] Droval, G.;   Feller, J. F.;   Salagnac, P.; Glouannec, P., Thermal conductivity enhancement of electrically insulating syndiotactic poly(styrene) matrix for diphasic conductive polymer composites. *Polymers for Advanced Technologies* **2006,** *17* (9-10), 732-745.

[24] Ghorpade, R. V.;   Cho, D. W.; Hong, S. C., Effect of controlled tacticity of polyacrylonitrile (co)polymers on their thermal oxidative stabilization behaviors and the properties of resulting carbon films. *Carbon* **2017,** *121*, 502-511.

[25] Zhang, T.; Luo, T., Role of Chain Morphology and Stiffness in Thermal Conductivity of Amorphous Polymers. *The Journal of Physical Chemistry B* **2016,** *120* (4), 803-812.

[26] Bai, L.;   Zhao, X.;   Bao, R.-Y.;   Liu, Z.-Y.;   Yang, M.-B.; Yang, W., Effect of temperature, crystallinity and molecular chain orientation on the thermal conductivity of polymers: a case study of PLLA. *Journal of Materials Science* **2018,** *53* (14), 10543-10553.

[27] Ma, H.;   Ma, Y.; Tian, Z., Simple Theoretical Model for Thermal Conductivity of Crystalline Polymers. *ACS Applied Polymer Materials* **2019,** *1* (10), 2566-2570.

[28] Cho, B.-G.;   Joshi, S. R.;   Lee, J.;   Park, Y.-B.; Kim, G.-H., Direct growth of thermally reduced graphene oxide on carbon fiber for enhanced mechanical strength. *Composites Part B: Engineering* **2020,** *193*.

[29] Miyake, K.;   Satomi, N.; Sasaki, S., Elastic modulus of polystyrene film from near surface to

bulk measured by nanoindentation using atomic force microscopy. *Applied Physics Letters* **2006,** *89* (3).

[30] Giddings, V. L.; Kurtz, S. M.; Jewett, C. W.; Foulds, J. R.; Edidin, A. A., A small punch test technique for characterizing the elastic modulus and fracture behavior of PMMA bone cement used in total joint replacement. *Biomaterials* **2001,** *22* (13), 1875-1881.

[31] Chang, C.; Muccio, D. D.; St. Pierre, T., Determination of the tacticity and analysis of the pH titration of poly(acrylic acid) by proton and carbon-13 NMR. *Macromolecules* **1985,** *18* (11), 2154-2157.

[32] Ishitake, K.; Satoh, K.; Kamigaito, M.; Okamoto, Y., Stereospecific Free Radical and RAFT Polymerization of Bulky Silyl Methacrylates for Tacticity and Molecular Weight Controlled Poly(methacrylic acid). *Macromolecules* **2011,** *44* (23), 9108-9117.

[33] Couvreur, L.; Lefay, C.; Belleney, J.; Charleux, B.; Guerret, O.; Magnet, S., First Nitroxide-Mediated Controlled Free-Radical Polymerization of Acrylic Acid. *Macromolecules* **2003,** *36* (22), 8260-8267.

[34] Xie, X.; Li, D.; Tsai, T.-H.; Liu, J.; Braun, P. V.; Cahill, D. G., Thermal Conductivity, Heat Capacity, and Elastic Constants of Water-Soluble Polymers and Polymer Blends. *Macromolecules* **2016,** *49* (3), 972-978.

[35] Han, W.; Bai, Y.; Liu, S.; Ge, C.; Wang, L.; Ma, Z.; Yang, Y.; Zhang, X., Enhanced thermal conductivity of commercial polystyrene filled with core-shell structured BN@PS. *Composites Part A: Applied Science and Manufacturing* **2017,** *102*, 218-227.

[36] Stuart, B., Polymer analysis. **2010**.

[37] Kazantsev, M. S.; Beloborodova, A. A.; Frantseva, E. S.; Rybalova, T. V.; Konstantinov, V. G.; Shundrina, I. K.; Paraschuk, D. Y.; Mostovich, E. A., Methyl substituent effect on structure, luminescence and semiconducting properties of furan/phenylene co-oligomer single crystals. *CrystEngComm* **2017,** *19* (13), 1809-1815.

[38] Feng, H.; Cheng, R.; Zhao, X.; Duan, X.; Li, J., A low-temperature method to produce highly reduced graphene oxide. *Nat Commun* **2013,** *4*, 1539.

VII. Acknowledgements